AD-A131 001 NUMERICAL SIMULATION OF HIGH ENERGY LIGHT ION BEAM FLOW 1/1
THROUGH A FOILLESS DIODE(U) NAVAL RESEARCH LAB
WASHINGTON DC R J BARKER ET AL. 21 JUL 83 NRL-MR-5058

UNCLASSIFIED F/G 12/1 NL

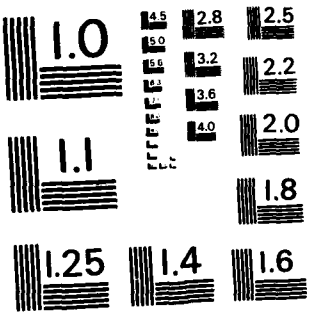

SECURITY CLASSIFICATION OF THIS PAGE (When Data Entered)

REPORT DOCUMENTATION PAGE	READ INSTRUCTIONS BEFORE COMPLETING FORM
1. REPORT NUMBER: NRL Memorandum Report 5058	2. GOVT ACCESSION NO.: AD-A131 CK1
	3. RECIPIENT'S CATALOG NUMBER
4. TITLE (and Subtitle): NUMERICAL SIMULATION OF HIGH ENERGY LIGHT ION BEAM FLOW THROUGH A FOILLESS DIODE	5. TYPE OF REPORT & PERIOD COVERED: Interim report on a continuing NRL problem.
	6. PERFORMING ORG. REPORT NUMBER
7. AUTHOR(s): R.J. Barker,* C.W. Robersont and F.M. Mako@	8. CONTRACT OR GRANT NUMBER(s)
9. PERFORMING ORGANIZATION NAME AND ADDRESS: Naval Research Laboratory, Washington, DC 20375	10. PROGRAM ELEMENT, PROJECT, TASK AREA & WORK UNIT NUMBERS: 61153N; RR0110941; 47-1484-0-3
11. CONTROLLING OFFICE NAME AND ADDRESS: Office of Naval Research, Arlington, VA 22217	12. REPORT DATE: July 21, 1983
	13. NUMBER OF PAGES: 22
14. MONITORING AGENCY NAME & ADDRESS(if different from Controlling Office)	15. SECURITY CLASS. (of this report): UNCLASSIFIED
	15a. DECLASSIFICATION/DOWNGRADING SCHEDULE

16. DISTRIBUTION STATEMENT (of this Report)

Approved for public release; distribution unlimited.

17. DISTRIBUTION STATEMENT (of the abstract entered in Block 20, if different from Report)

18. SUPPLEMENTARY NOTES

*Present Address: Mission Research Corp. Alexandria, VA
†Present Address: JAYCOR, INC. Alexandria, VA
@Present Address: Office of Naval Research, Arlington, VA

19. KEY WORDS (Continue on reverse side if necessary and identify by block number)

Numerical Simulation
Foilless Diode
Intense Relativistic Electron Beams
Intense Ion Beams
Collective Ion Acceleration

20. ABSTRACT (Continue on reverse side if necessary and identify by block number)

A numerical and theoretical study is reported which treats the effects upon a 500 keV, hollow electron beam in a foilless diode along the centerline of which has been injected a beam of 30 MeV protons. Specifically, the results of simulations of three, separate equilibrium diode states (for electron-only, 1 kA of protons, and 5 kA of protons) are reported. The computational findings are compared to rough, theoretical predictions and very good agreement is observed. The conclusion may be drawn that, for the diode parameters studied, a 1 kA beam of 30 MeV protons

(Continued)

DD FORM 1 JAN 73 1473 EDITION OF 1 NOV 65 IS OBSOLETE
S/N 0102-014-6601

SECURITY CLASSIFICATION OF THIS PAGE (When Data Entered)

20. ABSTRACT (Continued) (relativistic electron beams)

does not seriously disrupt the electron beam. On the other hand, a 5 kA proton beam not only radically alters the REB characteristics but also itself falls prey to strong, radial ballooning.

CONTENTS

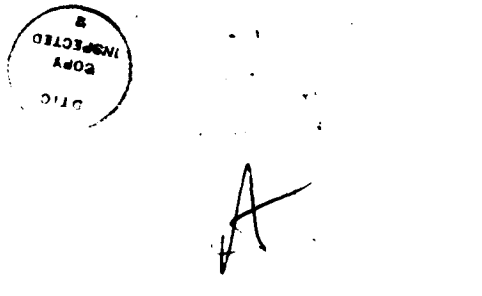

NUMERICAL SIMULATION OF HIGH ENERGY LIGHT ION BEAM FLOW THROUGH A FOILLESS DIODE

I. INTRODUCTION

Interest remains high in the quest for a compact, high energy, intense light-ion beam accelerator. Some of the areas of application for such an accelerator include directed energy systems, inertial confinement fusion drivers and magnetic fusion fuel injectors. The desired operating parameters for such an accelerator are an ion energy of from 0.1 to 1 GeV, a beam intensity of from 10^{13} to 10^{16} ions/cm^2 per pulse, and a pulse length of from less than one nanosecond to a millisecond. To be termed "compact," the device should not measure more than 10 to 30 meters in any dimension.

The ability to generate intense relativistic electron beams (IREB's) in foilless diodes[1,2] has brought the concept of a compact ion accelerator very close to a reality in the form of collective ion accelerators (CIA's). These collective accelerators have received much attention over the years.[3–6] Their operation relies upon the existence of localized, collective field gradients in excess of 1 MV/cm in an IREB. In comparison, conventional accelerators provide electric fields on the order of only 0.01 MV/cm which is unacceptable for a "compact" device. Although many approaches exist for achieving the acceleration of positive ions via the collective electric field produced by an intense relativistic electron beam, not all approaches can be scaled-up to achieve high ion energies. Scaleability implies a systematic procedure for maintaining synchronization between the ion being accelerated and its accelerating electrostatic potential well. This requirement of scaleability may be generalized to any type of accelerator.

The "space charge wave accelerator" concept has been proposed at NRL to achieve such scaleability.[7] The fundamental idea behind the concept is the sustained matching of ion beam velocity with the phase velocity of the accelerating IREB space charge wave along the entire length of the CIA (collective ion accelerator). The most formidable challenge to this concept is the matching of injected ion beam velocity with the minimum electron space charge wave velocity. Technical restraints appear to place a lower limit of 0.2-0.3 c on the phase velocity of the fundamental mode of a 1 MeV IREB space charge wave. This dictates an injected proton energy of 16-30 MeV. If that synchronization of initial velocities can be met, the geometry of the accelerator cavity can be designed to keep v_{ion} and v_{phase} in step. The specific design used is termed the Converging Guide Accelerator or CGA.[8] The phase velocity of the wave in a conducting cylinder depends on the ratio of beam to wall radii. The phase velocity increases inversely with this ratio. Thus, the wave can be accelerated by accelerating the beam. The beam can be accelerated by passing it through a metal tube with a converging radius.

In Fig. 1, ions are injected from the right along the central axis of the electron beam which is also propagating from right to left. Next, a space charge wave is excited and grows around the ions. The ions loaded into the wave are accelerated by it as it too accelerates in step. The electron beam is then dumped and the ions extracted from the far left. Two meters of magnetic field at a strength of 20 kG are required for this system. Initially, the electron beam planned for use with this system will have an energy of 0.5 MeV and a current of 1.4 kA for 250 nsec. Also, the electron beam generator can be operated at 10 pulses per second. The trace that is shown in Fig. 1 is a photograph of the machine voltage versus time. The high voltage machine was used in conjunction with a resistive load. For proof-of-principle testing, low-current, 30 MeV proton beams could be injected from a conventional ion accelerator such as the cyclotron at NRL.

Manuscript approved March 28, 1983.

Such a low ion current experiment can indeed test the wave accelerator concept but there remains another question to be answered before kiloamp-level, injected beam devices are constructed. What are the consequences of injecting into a foilless diode a 30 MeV proton beam of comparable amperage to the current normally carried by the electrons alone in the diode. How will the structure of the potential well inside the hollow electron beam be effected? Will the net electron current flowing through the diode increase and, if so, by how much? These are the matters addressed by the computational research reported herein. The findings demonstrate that an injected 30 MeV proton beam carrying 10% of the normal diode electron current will not seriously effect the potential well structure in or the electron current of the foilless diode. A five-fold increase in the ion beam current, on the other hand, destroys the well and doubles the electron current. Thus, clearly "safe" and clearly "unsafe" ion current levels have been established. The determination of an exact "critical" ion current for use in the CGA device is not important at this time and has been left for future research.

In the section that follows, the actual physical device to be simulated is described in detail. Section III then outlines the key characteristics of the DIODE2D computer code which was used to conduct the numerical simulation. The numerical results are presented in Section IV including such information as radial profiles of beam current density and plots of the electrostatic potential well structure in the diode. In order to give added emphasis and understanding to the numerics, Section V is devoted to a simple theoretical analysis of the physics of the ion beam and diode. Good agreement is found between the theoretical predictions and the numerical findings. Finally, Section VI summarizes the major conclusions that can be drawn from this work and suggests material for future research.

II. THE FOILLESS DIODE

The physical diode designed for the experimental testing of this new CGA concept closely resembles that shown in Fig. 2. It corresponds roughly to the "wave growth" section of the accelerator shown in Fig. 1. The coaxial, vacuum, power feed line tapers inward radially as it traverses the axial length of the near-conical cathode. The tip of the cathode coincides with the entrance plane of a long (>1 meter) cylindrical drift tube. The outer radius of the cathode is about 1.5 cm. A hole 0.5 cm in radius is bored through the center of the cathode to serve as the injection port for the high energy ion beam. The coaxial, conical $A-K$ gap has a length of about five centimeters. The drift tube is given an inner radius of about 1.7 cm. The entire apparatus is immersed in a uniform axial magnetic field of about 10 kilogauss.

Ideally, the model diode to be numerically simulated would correspond exactly to that depicted in Fig. 2. Unfortunately, the simulation code, DIODE2D, which was used in these studies was incapable of efficiently handling that specific geometry. Particularly troublesome are the sloped walls of the cathode and of the coaxial power feed line as well as the overall meter-long length of the physical system. The existing code was capable of treating only conducting surfaces and boundaries which are strictly radial or strictly coaxial (i.e., they must have a rectangular $R-Z$ cross-section). Thus, a cylindrical cathode shank of some finite thickness must be substituted for the conical one. Furthermore, a combination of limited resolution and finite computer data storage capabilities prohibits the accurate treatment of a system less than 2 cm in radius but over 100 cm long. The total axial length of the model system will be shortened instead to 10 cm. The peculiarities of the Poisson-solver for the electric and magnetic potentials in that system also required that the tube be terminated by a fixed-potential, conducting wall.[9] The final approximation to the original system took the form shown in Fig. 3.

The cathode used in the numerical model is a hollow cylinder 1.2 cm in radius with a shank wall thickness of 0.4 cm. It projects axially 2.5 cm into the 10.0 cm long drift-tube (anode). The anode tube inner radius is at 1.7 cm. This leaves a radial $A-K$ (anode-cathode) gap of 0.5 cm which very comfortably exceeds the 0.17 cm gyroradius of a 0.5 MeV electron in a 10 kG magnetic field. Analysis using existing theory[10-12] leads to estimates of foilless diode electron beam currents of 8-10 kA or diode

power levels of 4-5 GW. Along the central axis of this device will be injected a 0.7 cm radius beam of 30 MeV protons. Three separate simulations were conducted of this configuration. The first was a "benchmark" run to determine the normal, electrons-only operating characteristics of the foilless diode. Of importance is not only the gross e-beam current but also the beam profile and the structure of the electrostatic potential well inside the beam. The final two simulations were conducted with the high-energy proton beam flowing through the device. Specific ion beam currents of 1 kA and 5 kA were chosen for these two test cases.

III. NUMERICAL IMPLEMENTATION

A modified, electrostatic-magnetostatic version of NRL's DIODE2D computer code was used to carry out the simulations. The details of the code may be found elsewhere.[13] It is sufficient here to note that the code is 2-1/2-dimensional in that it explicitly moves particles in R and Z (radially and axially) in space while keeping track of all three components of their canonical momentum. The treatment is fully relativistic for both electrons and protons. Unlike a full electromagnetic simulation code, DIODE2D is designed to find only equilibrium charge, current, and field configurations in the device under study.

Particle contributions to net charges and currents as well as the resulting E and B field values are stored in a mesh of discrete data points covering the entire diode. The spacing between data points was fixed at $R = 0.05$ cm radially and $Z = 0.078$ cm axially. This allowed for 34 data cells to span the 1.7 cm from the centerline to the inner radius of the anode tube and 128 cells from the back of the cathode to the anode endplate. The protruding cathode shank measured 8 data cells thick and 32 cells long. On its front face, electron emission was permitted from the outer 7 of the 8 possible emission points. The eighth cell was not allowed to emit in order to obtain additional numerical accuracy in the field values governing electron emission from the inside lip of the cathode shank. Emission was permitted all along that inner, as well as the outer shank surface except for the rearmost 6 cells.

The magnitude of the electron emission from a given cathode surface is determined by the amount of space charge necessary to zero out the perpendicular component of the electric field at the emission point. In order to simulate the injection of the 30 MeV proton beam of predetermined amperage, the inner 14 cells of the cathode endplate inside the shank were designated as proton "emission" points. The emission at those points, however, was completely independent of the adjacent electric field values. A constant, emitted current density, J_i, of 0.65 kA/cm^2 was imposed for the 1 kA beam case and 3.25 kA/cm^2 for the 5 kA case at each of the 14 points. Particles of both species were perfectly absorbed upon hitting any of the boundary surfaces, including the surfaces of the protruding cathode shank.

All quantities of interest in the device were monitored by the computer code's extensive diagnostics. Electron and ion, emitted and collected current densities were recorded over all relevant surfaces. Electrostatic equipotential contour lines and magnetic field lines throughout the device were plotted. Sample values of all three components of the magnetic field are similarly recorded. Net charges and currents were periodically listed. Finally, the positions of statistical samplings of electrons and protons were plotted at equilibrium.

IV. RESULTS

First, a "benchmark" simulation was run in which only electrons were allowed in the diode. In agreement with theory (see Section V), a net electron current of 9.6 kA was measured. Of that total amount, 2.8 kA was emitted from the face of the cathode shank tip while the remaining 6.8 kA originated from the outside surface of the shank. Emission from the inner shank surface was negligible. A net electron charge of -1.86×10^4 statcoulombs was found to be in the system. Figure 4 presents a

plot of sample electron positions at equilibrium. Of note is the waviness of the outer envelope of the electron beam. Similar beam behavior was observed in foilless diode simulations conducted by R. Jackson[14,15] and others. The electrostatic potential contour plot for the device modeled in simulation is shown in Fig. 5. The beam envelope waviness is mirrored in these equipotentials. It is also clear from this figure that the electric field inside the hollow cathode is negligible, in agreement with the vanishingly small electron emission observed there. It also appears that electrons leaving the cathode are fairly rapidly accelerated to the 40% equipotential (0.2 MeV) before entering a virtual "drift region" about 3.5 cm long starting about 2.0 cm downstream of the cathode tip. Electron energy and velocity are nearly constant in this region as would be the case in an actual full-length foilless diode drift tube. It is therefore that region where beam behavior will most closely mimic a realistic device. Finally, the self-magnetic field lines generated by the *e*-beam are depicted in Fig. 6. Imposed over this self-field pattern is the uniform 10 kG background field. Up to about $Z = 8.5$ cm, the beam field is diamagnetic in nature, lowering the inside, imposed B_Z by about 40-80 gauss and intensifying the field near the anode tube by a like amount. The self-field between $Z = 8.5$ and 10.0 cm, where electrons receive a final 0.3 MV of acceleration, is of the opposite orientation. However, that region as well can boast of only 50-100 gauss field strengths.

The second case to be tested was that involving the 1 kA, 30 MeV proton beam injected in the manner described in the previous section. The net electron current in the new equilibrium increased by 2 kA to 11.6 kA. Of that total current, 4.3 kA was being emitted from the tip (compared to 2.8 kA for the electrons-only case), 0.4 kA were coming from the inner shank surface, while the outer shank surface emission remained practically unchanged at 6.9 kA. The ion beam had introduced a total charge of $+4.06 \times 10^3$ statcoulombs into the diode while the electron charge had increased to -2.11×10^4 statcoulombs. Thus, the electron beam characteristics of the diode itself had changed very little. In addition, the ion beam envelope experienced virtually no ballooning. This is evident from Fig. 7 which presents the steady-state ion beam envelope superimposed over the sample electron position plot. The qualitative character of the hollow electron beam has likewise remained essentially unchanged. The first truly major change manifests itself in the equipotential plot of Fig. 8. Comparison with Fig. 5 shows the distortions caused by the concentration of positive space charge along the axis. The contours are sucked into the hollow cathode up to the 40% potential. This accounts for the turn-on of electron emission there. Also, electrons reaching the previously-mentioned "drift region" between $Z = 4.5$ to $Z = 8.0$ cm are now at about 0.25 MeV instead of the 0.20 MeV of the electrons-only case. Finally, Fig. 9 shows the changes made to the self-magnetic field lines generated by the electron beam. The magnitudes of those fields in the drift region remain unchanged in the range of 40 to 80 gauss, but the orientation of the field has reversed. The imposed B_Z is now strengthened inside the beam and weakened outside. Although this effect is interesting, the small field strengths make it unimportant to the operation of the diode.

For the third and final test case, the current of the 30 MeV proton beam was increased to 5 kA. The steady state electron current rose to 19.7 kA with 8.3 kA from the shank face, 4.7 kA from its inner surface, and an outer shank emission current almost identical to the previous two cases at 6.7 kA. Of course, the ion charge increased by the same factor of five as its current to $+2.04 \times 10^4$ statcoulombs. In partial compensation, the net electron charge had grown to -3.32×10^4 statcoulombs. Clearly the normal operation of the foilless diode has been seriously disrupted. Its electron current has more than doubled. Even more dramatic is the destruction of the ion beam. This is illustrated by the equilibrium sample particle plot of Fig. 10. The proton beam envelope has expanded halfway through the width of the hollow electron beam by the time it arrived at the end of the drift tube. Similarly the electrostatic potential contours shown in Fig. 11 no longer bear much resemblance to the ion-free case of Fig. 5. Electrons now experience almost 80% of the total diode potential increase before entering the "drift region." There no longer exists any effective "potential well" through which the proton beam can travel. Finally, the self-magnetic field of the electrons (see Fig. 12) can no longer be ignored. Its drift region magnitudes now range from about 200 to 700 gauss which is an appreciable fraction of the

imposed 10 kG field. As in the 1 kA ion beam case, this self-field strengthens the B_Z along the axis and weakens it outside the *e*-beam radius.

The major results of the above three simulations are summarized in Table 1. The statement can be made that the injection of a 1 kA, 30 MeV proton beam along the axis of the foilless diode being studied, does not seriously disrupt the normal operating characteristics of the device. The injection of a 5 kA, 30 MeV ion beam does cause serious disruption. Correspondingly, the 1 kA beam is virtually uneffected by its passage through the diode, while the 5 kA beam undergoes severe ballooning. In order to better understand these macroscopic results, it is important to examine the modifications made by each case on the individual current density profiles of each case. Figure 13 depicts the radial profiles of the electron current density, J_e, emitted from the tip face of the cathode shank. The profiles all have a characteristic double-pronged shape.[14] They show that for this diode the doubling of the emitted currents on this surface is predominantly occurring at the points of lower radius. Those points are closer to the ion beam, whose space-charge has grossly distorted the electric field values there. From Fig. 14, however, it is obvious that the electron emission from both the inner and the outer shank surfaces are virtually identical for the electrons-only and the 1 kA beam case. Since some 70% of the total diode current originates on the outer surface, this agrees with the overall close similarity between the two cases. The 5 kA beam case is quite a different matter. Although the net outside shank emission is about the same as the previous cases, the axial profile of J_e is grossly depressed over the front half of the shank and mildy enhanced over the rear half. This is a manifestation of the 2 1/2-fold increase in the value of B_θ along that surface. The near-normal amount of negative charge emitted from the rear half is prevented from leaving the near vicinity of the shank as it travels toward the front face. This negative space charge then impedes the electron emission along the front half of that surface. The most dramatic change, however, is in the inner shank surface emission. For the 5 kA beam case, the emission there rivals that of the outside surface. For the other two cases that inner surfaces had been effectively non-emitting. The combined emission changes are all reflected in the radial profiles of electron current densities collected at the anode face (Z = 10 cm). These are shown in Fig. 15. In addition to the overall enhancement of collected current from case to case, a distinct pinching of the beam toward the central axis can be seen. This is to be expected due to the increased self-magnetic field strength but the magnitude of the radial displacement of the mean current density is limited by the imposed 10 kG axial *B*-field.

The final diagnostic measured the radial profiles of the 30 MeV proton beam in the plane located at Z = 7.5 cm, well inside the electron beam "drift region." Two profiles are shown for the 1 kA beam case in Fig. 16. The first represents the initial, imposed beam profile a mere 50 timesteps ($\Delta t = 2 \times 10^{-12}$ sec) after the beginning of the simulation. The other profile shows the modest spread of the beam about 0.8 nano-seconds later. The change is quite negligible, indicating excellent confinement and stability of the beam. Once again, the 5 kA case is dramatically different. The corresponding profiles for that high current beam are shown in Fig. 17. Over the same 0.8 nanosecond period, this beam has expanded from its initial 0.7 cm radius to over 1.0 cm, well beyond the inner cathode shank radius and the inner radius of the hollow electron beam. That configuration is clearly unstable.

V. THEORY COMPARISON

In this section analytic expressions are derived and compared to the simulation results. The two major results are the radial ballooning of the ion beam and the increase in the electron limit current as the ion current is increased. Agreement between theory and computation is quite good.

The radial equation of motion for the ions decouples and only the ion beam's self fields determine the ion motion. This is true for times that are short in comparison to the axial gyro-period. That is, $t^2 << \Omega_z^{-2}$, where, $\Omega_z = \frac{qB_z}{\gamma_M}$ and B_z is the axial magnetic field. Also, for $\beta^2 << 1/2$, where β is

the ion velocity divided by the speed of light, then changes in the relativistic mass factor can be neglected. With these assumptions the equation of motion for the ions at the beam surface is given by

$$\gamma M \frac{d^2 r}{dt^2} = qE_r - qV_z B_\theta \tag{1}$$

where: q and M are the ion charge and mass, E_r and B_θ are the self electric and magnetic fields in the ion beam, γ is the relativistic mass factor, V_z is the axial ion velocity, and r is the radial position of ions at the beam surface. Assuming current conservation Eq. (1) reduces to[17]

$$\frac{d^2 r}{dt^2} = \frac{k}{r} \tag{2}$$

where: $k = \dfrac{qI}{2\pi\epsilon_0 M V_z \gamma^3}$, I is the ion beam current, and ϵ_0 is the dielectric constant of free space. Equation (2) can be solved in series form[18] to give,

$$\sum_{n=0}^{\infty} \frac{\{\ln(r/r_0)\}^{n+1/2}}{(2n+1)\,n!} = \frac{\sqrt{k/2}}{r_0}\, t, \tag{3}$$

where: r_0 is the initial beam radius at $t = 0$ and r is the final radius at time t. In Table 2, a comparison is made between the code time, t, to reach the final radius, r, and the time calculated by Eq. (3). This comparison is made for 30 MeV protons.

It is clear from the comparison that the self fields of the ion beam determine its motion. Of the self fields, the electric field dominates in the expansion. This result does not limit the maximum ion current. Since, the ion beam expands to the diameter of the electron beam, it's electric field is reduced thus allowing for more ion current to flow. Increasing the ion current then increases the electron limit current which in turn allows for an increase in the ion current, etc.

In addition to the problem of ion beam ballooning, the simulation also addressed the major question of changes in the diode's electron current due to the presence of the ion beam. The maximum electron current is determined by the potential distribution along the electron-emitting cathode surfaces. When ions are present the potential is raised and hence the limit current is increased.

In Fig. 18 electrons and ions are moving in the same axial direction. A large external magnetic field is applied in the direction of particle motion, z. This field is large enough to magnetize the electrons but not the ions. Furthermore, the assumptions are made that (a) J_e and J_i are uniform, (b) $|B_{\theta i}|$ and $|B_{\theta e}| \ll |B_z|$, (c) $|E_r| < |B_z|c$, and (d) Electron velocity shear can be neglected (where J_e and J_i are the electron and ion current density; $B_{\theta i}$, $B_{\theta e}$ and B_z are the ion, electron and external, magnetic fields; E_r is the radial ion electric field; c is the vacuum speed of light).

From Gauss' law the potential inside the electron beam, region 3, (see Fig. 20) is given by the expression,[19]

$$\phi(r) = \frac{I_i}{2\pi\epsilon_0 V_i} \ln(R/r) - \frac{I_e}{4\pi\epsilon_0 V_z}\left[\frac{r_2^2 - r^2}{r_2^2 - r_1^2} + 2\ln R/r_2 - \frac{2r_1^2}{r_2^2 - r_1^2}\ln(r_2/r)\right] \tag{4}$$

where I_i and I_e are the ion and electron current, V_i and V_z are the ion and electron velocity, and ϵ_0 is the permitivity of the free space. The quantity, ϕ, may be eliminated from Eq. (4) by using conservation of energy,

$$\frac{-mc^2}{e}(\gamma - \gamma_0) = \phi. \tag{5}$$

The maximum electron current can then be found by setting $\frac{dI_e}{d\gamma}$ to zero, thus yielding

$$I_e \leqslant \frac{\left[I_o(\gamma_0 - \gamma) + (2I_i/\beta_i) \ln\left(\frac{R}{r}\right)\right](1 - 1/\gamma^2)^{1/2}}{\left[\frac{r_2^2 - r^2}{r_2^2 - r_1^2} + 2 \ln R/r_2 - \frac{2r_1^2}{r_2^2 - r_1^2} \ln\left(\frac{r_2}{r}\right)\right]} \tag{6}$$

where

$$I_0 = \frac{4\pi\epsilon_0 mc^3}{e} \simeq 17 \text{ kA}, \tag{7}$$

$$\gamma = \left[\frac{2I_i}{\beta_i I_0} \ln\left(\frac{R}{r}\right) + \gamma_0\right]^{1/3}, \tag{8}$$

$mc^2\gamma_0$ is the initial electron energy, m and e are the electronic mass and charge, and β_i is the ion velocity normalized to the vacuum speed of light.

By inspecting the first term in Eq. (8) it is clear that the presence of the ion current raises the final electron energy. This energy increase plays only a small role in the limit current expression. The biggest ion effect arises in Eq. (4) where the potential is directly increased by an increase in the ion current.

The magnitude of the limiting electron current of Eq. (6) varies with the radial position, r. In general Eq. (6) should be integrated from r_1 to r_2 to give a current that is weighted by the changing potential across the beam. However, since the equation itself is only a simple approximation, seeking such extra "precision" would be pointless. Instead, Eq. (6) will be evaluated at different radii and the effects discussed. An upper bound to the limit current can be obtained by setting $r = r_2$ then Eq. (6) becomes

$$I_e \leqslant \left[\frac{I_0(\gamma - \gamma)}{2 \ln R/r_2} + \frac{I_i}{\beta_i}\right](1 - 1/\gamma^2)^{1/2}, \quad r = r_2. \tag{9}$$

This gives an upper bound to the limit current since all particles are experiencing the maximum potential near the wall. A comparison is made in Table 3. If Eq. (6) is evaluated at $r = r_1$ then the result is,

$$I_e \leqslant \frac{\left[I_0(\gamma_0 - \gamma) + 2\frac{I_i}{\beta_i} \ln(R/r_1)\right](1 - 1/\gamma^2)^{1/2}}{\left[1 + 2 \ln R/r_2 - \frac{2r_1^2}{r_2^2 - r_1^2} \ln(r_2/r_1)\right]}, \quad r = r_1. \tag{10}$$

Note that when no ions are present, this will give a lower bound to the limit current since all of the particles are exposed to a potential minimum. Table 4 shows a comparison of Eq. (10) with the code results. As expected, the theoretical prediction is well below the code findings for the case with no ion beam present. For the two cases with ion injection, however, the addition of positive space charge inside $r = r_1$, elevates the potential there to such a degree that for the 5 kA case it actually exceeds that observed in Table 3 for $r = r_2$. It is clear from both Table 3 and Table 4 that the comparison between simulation and theory is quite good, considering the theoretical approximations that were made. Thus a scaling law for the electron limit current dependence on the ion current can be inferred. This effect can have a major impact on wave phase velocity control for the space charge wave accelerator. For example if the injection current is fixed a change in the ion current will shift the wave phase velocity thus removing ions from wave synchronization. However, at high γ_0 and for modest ion currents the effect is small. For example, if $I_i/I_e = 0.1$ and $\gamma_0 = 7.0$,

$$\frac{\Delta\gamma}{\gamma_0} \equiv \frac{\gamma - \gamma_0^{1/3}}{\gamma_0} \tag{11}$$

$$= \frac{1}{\gamma_0^{2/3}} \left\{ \left[1 + \frac{2I_i}{\gamma_0 \beta_i I_0} \ln\left(\frac{R}{r}\right) \right]^{1/3} - 1 \right\}$$

$$< 0.01.$$

Thus, the two major code results have been explained. Analytic expressions have been derived for predicting these results and good agreement was found between theory and code results. The mechanism for ion ballooning has been shown to be due primarily to the self electric field of the ion beam. Increases in the electron limit current are shown to be associated with an increase in the ion current. As discussed, a coupling between the ion and electron currents can negatively impact on ion-wave synchronization for the space charge wave accelerator.

VI. CONCLUSIONS

The numerical simulations presented here give the first documented evidence that a high current, high energy light ion beam can be injected down the central axis of a conventional foilless diode without either seriously disturbing the operating characteristics of the diode or causing significant disruption of the ion beam itself. For the 4-5 GW foilless diode studied and for a proton energy of 30 MeV a beam current of 1 kA can easily be tolerated. Increasing the ion beam current to 5 kA leads to a general break-down of the beam-diode system. The precise current value between 1 kA and 5 kA at which system stability ceases remains to be found. At $\gamma > 7$ a ten percent ion current will cause less than a one percent variation in beam energy. This appears acceptable for collective wave accelerators.

REFERENCES

1. J. Chen and R.V. Lovelace, Phys. Fluids **21**, 1623 (1978).
2. M.E. Jones and L.E. Thode, Los Alamos Scientific Lab Report LA-UR-79-3107 (1979).
3. S.E. Graybill and J.R. Uglum, J. Appl. Phys. **41**, 236 (1970).
4. G.W. Kuswa, L.P. Bradley, and G. Yonas, IEEE Trans. N. S. **20**, 305 (1973).
5. F. Mako, Ph.D. Thesis, Univ. of California, Irvine.
6. D.D. Ryutov and G.V. Stupakov, Fizika Plazmy 2 No. 4 and 5 (1976).
7. C. Roberson and F. Mako, Bull. Am. Phys. Soc. **24**, 1001 (1979).
8. F. Mako, JAYCOR Final Report No. 320-80-002-FR (1980).
9. That serious shortcoming has been corrected in NRL's new PREMAS code which allows for open axial boundaries with "floating" potentials. See: R.J. Barker and S.A. Goldstein, Bull. Am. Phys. Soc. **26**, 921 (1981).
10. E. Ott, T.M. Antonsen, and R.V. Lovelace, Phys. Fluids **20**, 1180 (1977).
11. A.V. Agafonov, V.S. Voronin, A.N. Lebedev, and K.N. Pazin, Zh. Tekh. Fiz. **44**, 1909 (1974), [Sov. Phys. Tech. Phys. **19**, 1188 (1975)].

12. V.S. Voronin, E.G. Krastelev, A.N. Lebedev, and B.N. Yablokov, Fiz. Plazmy **4**, 606 (1978), [Sov. J. Plasma Phys. **4**, 336 (1978)].

13. R.J. Barker, A.T. Drobot, S.A. Goldstein, and R.E. Lee; *Proc. 9th Conf. on the Numerical Simulation of Plasmas*, Evanston, Illinois (1980).

14. R.H. Jackson and R.K. Parker, Bull. Am. Phys. Soc. **23**, 906 (1978).

15. R.H. Jackson, et al., Bull. Am. Phys. Soc. **25**, 947 (1980).

16. R.J. Barker, S.A. Goldstein, and R.E. Lee, NRL Memorandum Report 4279 (1980).

17. J.D. Lawson, *The Physics of Charged Particle Beams*, Clarendon Press, Oxford (1977).

18. I.S. Gradshteyn and I.W. Ryzhik, *Table of Integrals, Series and Products*, Academic Press, New York (1965).

19. R.B. Miller, *An Introduction to the Physics of Intense Charged Particle Beams*, Plenum Press, New York (1982).

Table 1 — Diode Currents and Charges

	Case 1	Case 2	Case 3
I_{ion} (kA)	0	1	5
$I_{electron}$ (kA)	9.6	11.6	19.7
I_{tip} (kA)	2.8	4.3	8.3
$I_{outside}$ (kA)	6.8	6.9	6.7
I_{inside} (kA)	—	0.4	0.7
Q_e (x1000 statcoul)	−18.6	−21.1	−33.2
Q_i (x1000 statcoul)	0	+4.06	+20.4

Table 2 — Comparison of Code and Analytic Calculated Times to Reach Final Radius

I_{ion} (kA)	1	5
r_0 (cm) initial	.725	.725
r (cm) final	.83	1.07
code time, $t(ns)$	.8	.8
time from Eq. (3), $t(ns)$	.859	.713
% Relative deviation in times	7.4	11

Table 3 — Comparison of Code and Analytic Limit Currents. Potential evaluated at $r = r_2$.

I_{ion} (kA)	0	1	5
$I_{electron}$ (kA) from Eq. (9)	11.03	13.49	24.13
$I_{electron}$ (kA) from Code	9.6	11.6	19.7
% Relative Deviation from Eq. (9)	12.7	14	18

Table 4 — Comparison of Code and Analytic Limit Currents. Potential evaluated at $r = r_1$.

I_{ion} (kA)	0	1	5
$I_{electron}$ (kA) from Eq. (10)	7.3	11.01	27.85
$I_{electron}$ (kA) from Code	9.6	11.6	19.7
% Relative Deviation from Eq. (10)	31.5	5.45	29

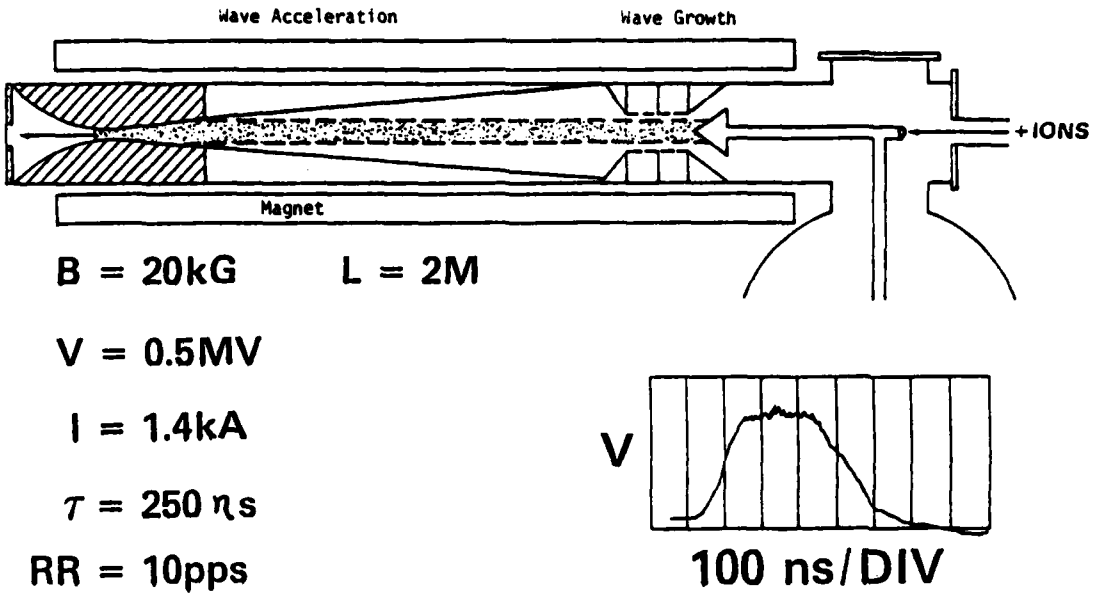

Fig. 1 — The converging guide accelerator

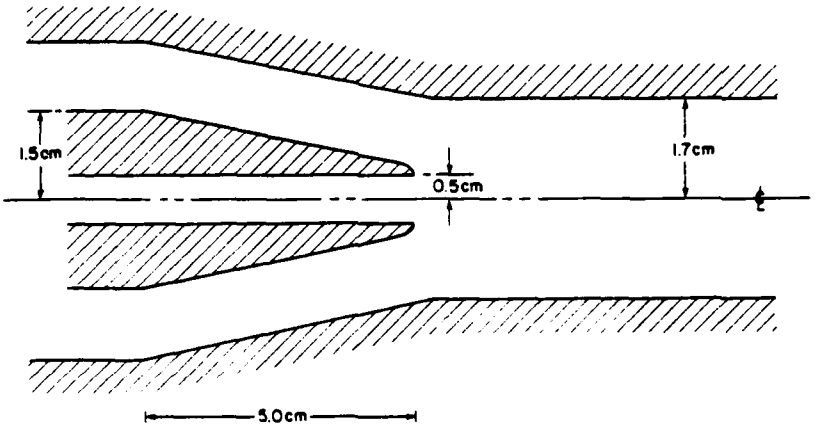

Fig. 2 — The experimental diode geometry

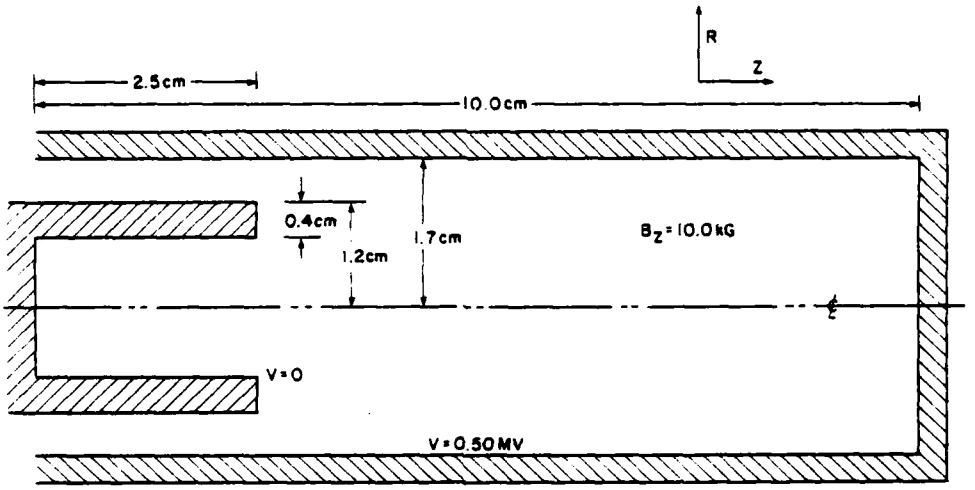

Fig. 3 — The numerical diode geometry

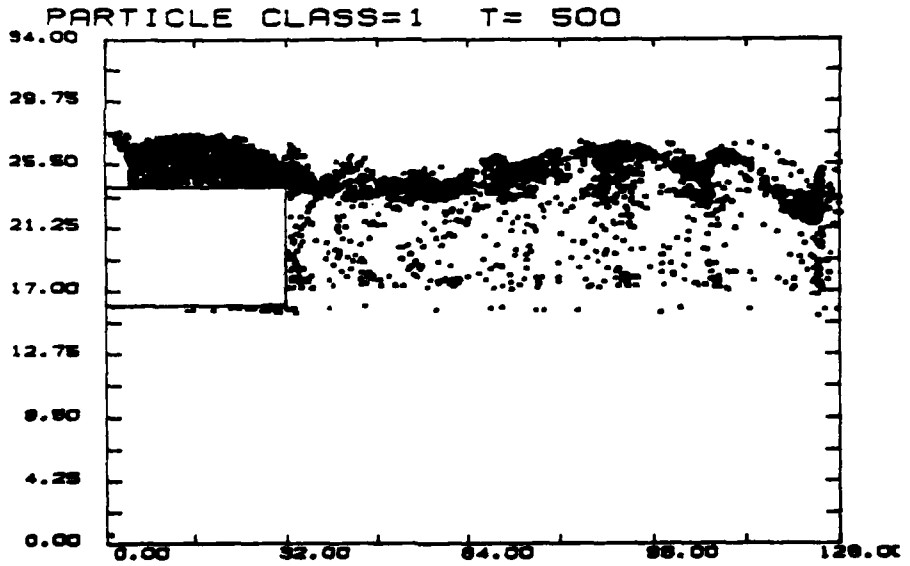

Fig. 4 — Sample electron positions in equilibrium diode with no ions present

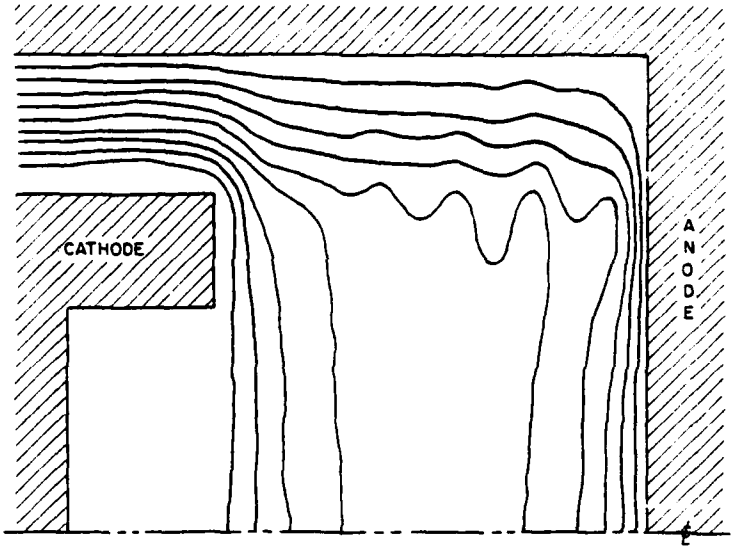

Fig. 5 — $\phi(r, z)$ for electrons—only diode

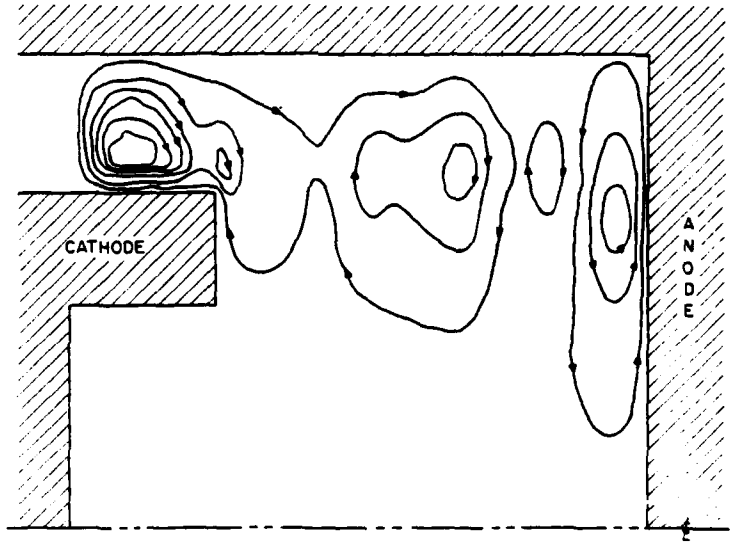

Fig. 6 — Self-magnetic field for electron—only diode

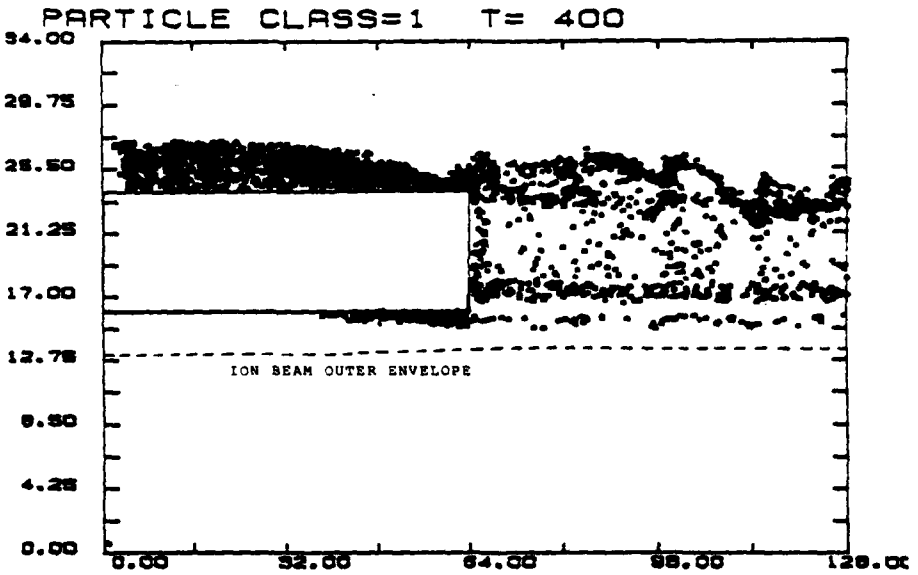

Fig. 7 — Steady-state sample electrons and ion beam envelope for 1 kA, 30 MeV proton beam

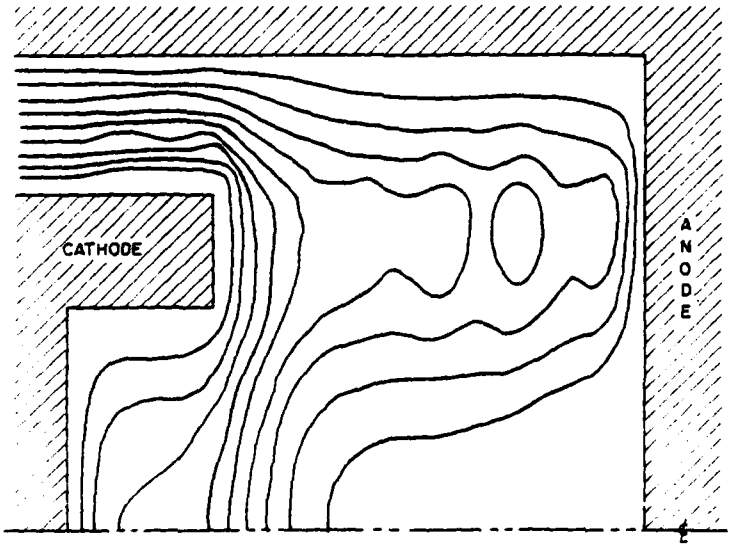

Fig. 8 — $\phi(r, z)$ for diode with 1 kA, 30 MeV proton beam

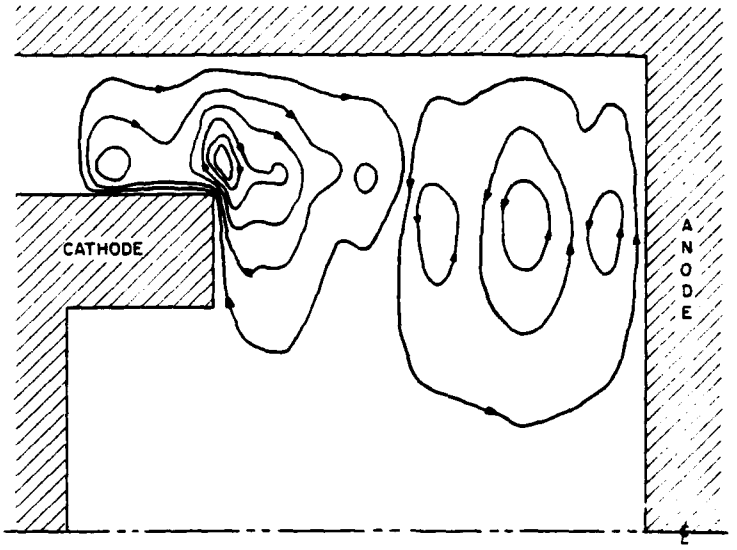

Fig. 9 — Self-magnetic field for diode with 1 kA.
30 MeV proton beam

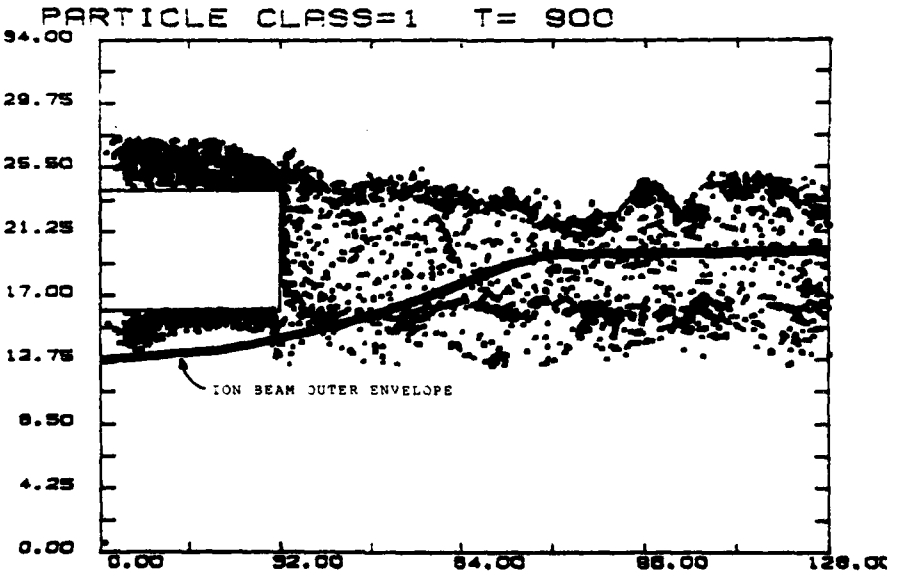

Fig. 10 — Sample electrons and ion beam envelope for 5 kA.
30 MeV proton beam

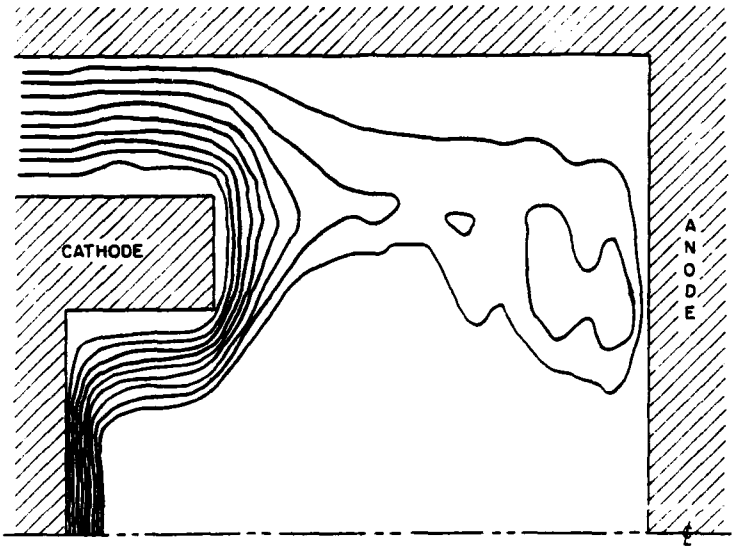

Fig. 11 — $\phi(r, z)$ for diode with 5 kA, 30 MeV proton beam

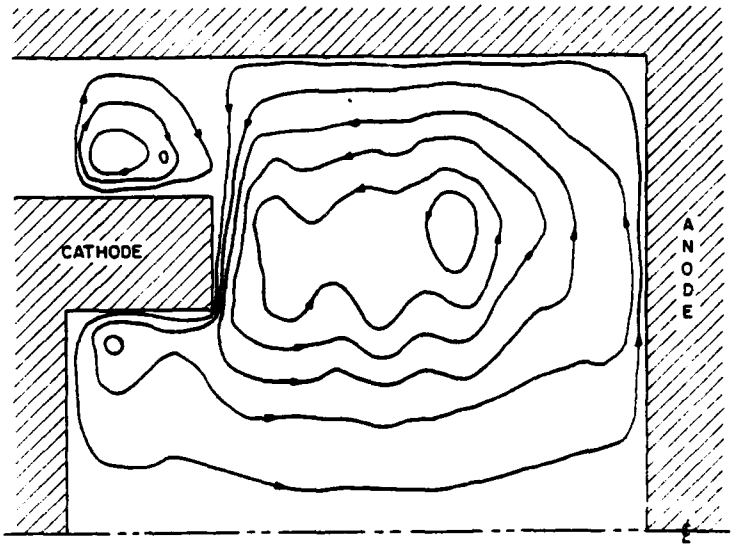

Fig. 12 — Self-magnetic field for diode with 5 kA, 30 MeV proton beam

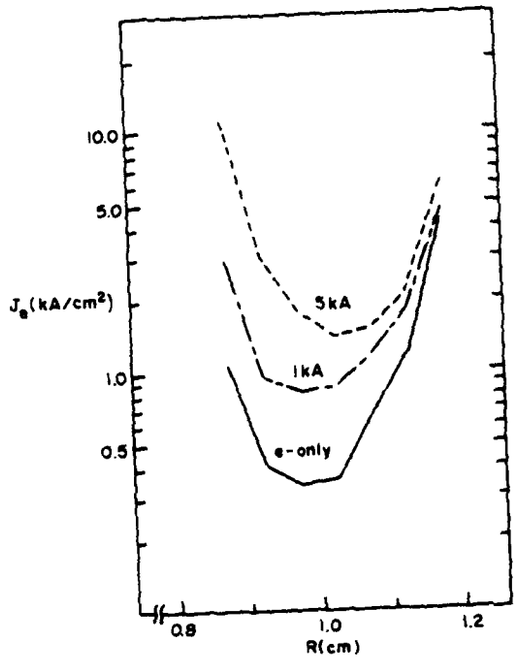

Fig. 13 — $J_e(r)$ emitted from cathode tip

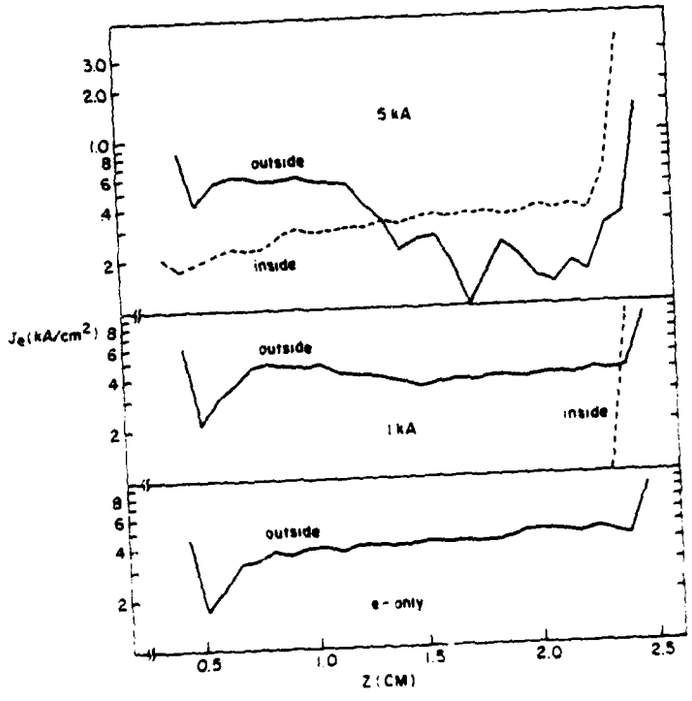

Fig. 14 — Profiles of electron shank emission

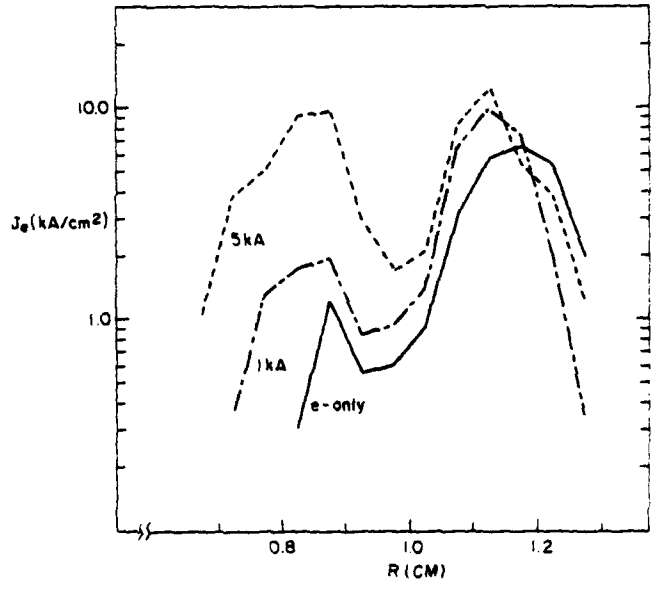

Fig. 15 — $J_e(r)$ collected at anode endplate

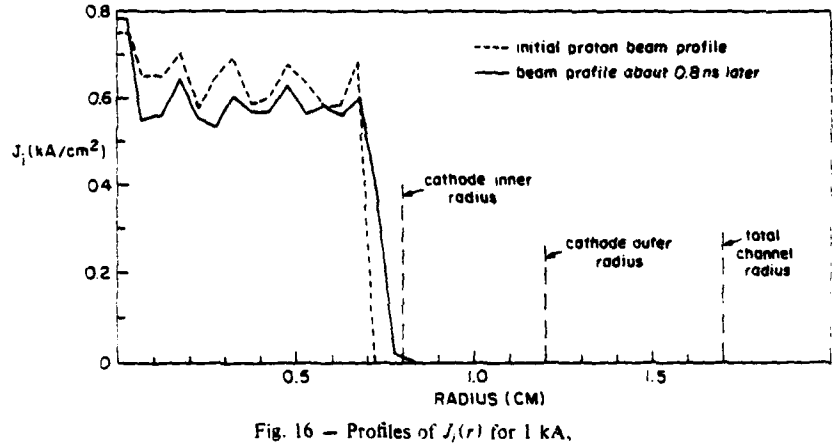

Fig. 16 — Profiles of $J_i(r)$ for 1 kA, 30 MeV proton beam case

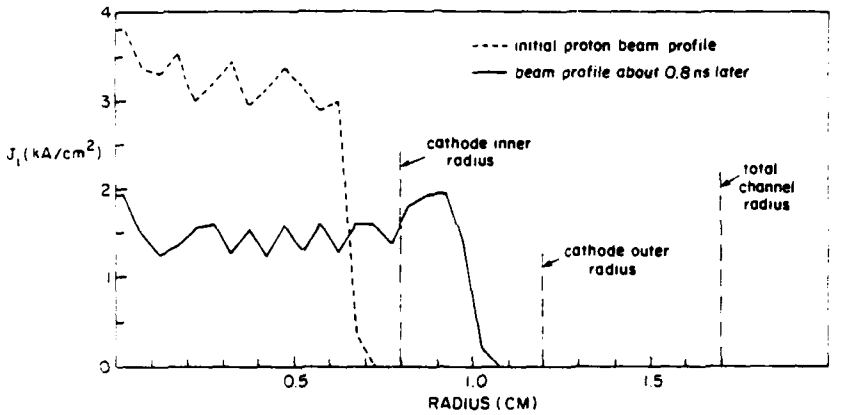

Fig. 17 — Profiles of $J_i(r)$ for 1 kA, 30 MeV proton beam case

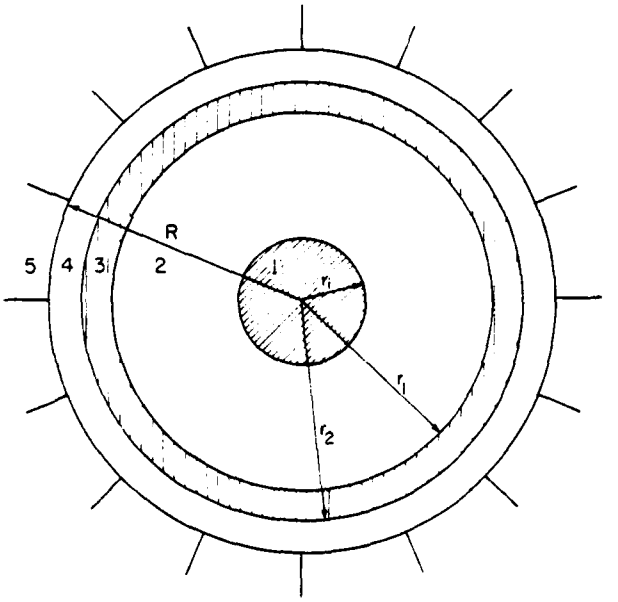

Fig. 18 — Schematic R-θ cross-section of foilless diode

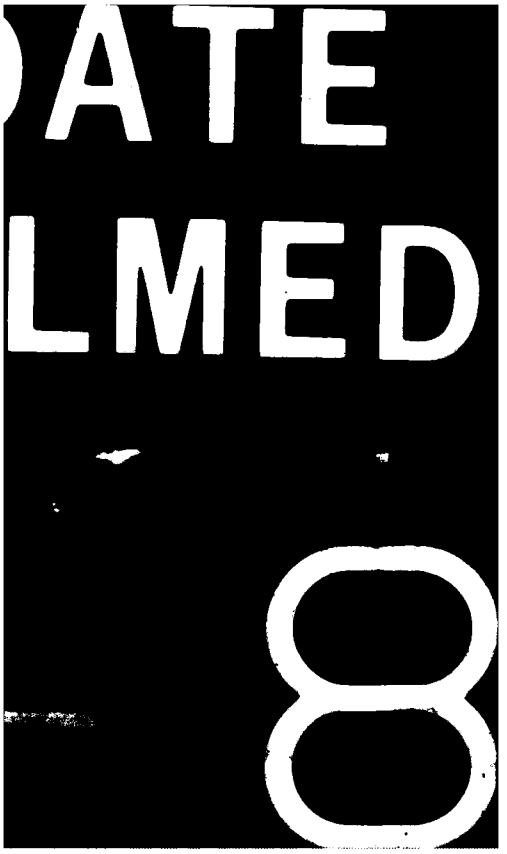
ATE
LMED
8